energy&fuels

pubs.acs.org/EF

Article

Surface Complexation Modeling of HPAM Polymer−Brine−Sandstone Interfaces for Application in Low-Salinity Polymer Flooding

Motaz Saeed and Prashant Jadhawar*

Cite This: https://doi.org/10.1021/acs.energyfuels.3c00542

Read Online

ACCESS | Metrics & More | Article Recommendations

ABSTRACT: Understanding the synergetic effects of wettability alteration by low-salinity waterflooding and mobility control by polymer flooding are important to assess the outcome of low-salinity polymer flooding in sandstone reservoirs. Moreover, investigating the interfacial chemical interactions within a polymer−brine−sandstone rock system allows for further understanding of the mechanistic mechanisms that dictate hydrolyzed polyacrylamide (HPAM) polymer's viscosity and adsorption on the sandstone surface. In this work, we utilize triple-layer surface complexation modeling in combination with the Derjaguin−Landau−Verwey−Overbeek (DLVO) theory to investigate the HPAM polymer−brine and sandstone−brine interactions that govern the polymer rheological properties. The ζ potential predicted from the proposed triple-layer model was used to investigate how salinity, polymer concentration, and temperature affect the viscosity of the HPAM polymer. We also propose the application of the novel concept of maximum energy barrier, calculated from the DLVO theory's interaction potential curve, as an indicator of polymer adsorption on the rock surface. Analysis revealed that polymer solution viscosity and ζ potential are potentially inherently correlated. Moreover, analysis results showed that the maximum energy barrier can indeed be used to predict the polymer adsorption on the rock surface. Analysis of the factors controlling polymer adsorption using the maximum energy barrier concept led to the conclusion that higher brine salinity and lower temperature result in higher polymer adsorption. This is explained by the reduction in the energy barrier when higher brine salinity and lower temperature are encountered, which results in lower system stability leading to higher attraction between the polymer chains and the rock surface.

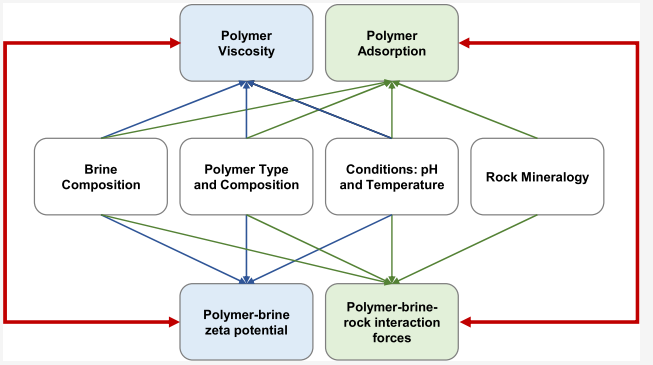

1. INTRODUCTION

In recent years, the idea of combining low-salinity waterflooding (LSWF) with other enhanced oil recovery (EOR) methods has been explored. Many research studies were conducted to evaluate the effectiveness of combining LSWF with other methods such as polymer flooding, surfactant flooding, gas injection, and hot waterflooding. This combination allows us to make use of the working mechanisms behind LSWF such as wettability alteration in synergy with other EOR mechanisms i.e., oil viscosity reduction, interfacial tension (IFT) reduction, and mobility control.[1−5] Mechanisms other than wettability alteration have been used to explain the low-salinity effect, such as fines migration, multicomponent ion exchange (MIE), pH increase and alkali-like effect, oil desorption, and electrical double-layer expansion among other mechanisms,[6−10] however, in this work wettability alteration is assumed to be the main mechanism.

Combining low-salinity waterflooding with gas injection can be conducted in different modes such as water alternating gas (WAG) and simultaneous water alternating gas (SWAG). Experimental studies show that LSWF coupled with gas injection results in a reduction in oil viscosity due to better gas solubility, leading to higher oil recovery in comparison with continuous gas injection.[1] Jiang et al.[11] studied this synergetic effect by injecting both LSW and miscible gas into a sandstone core sample in a WAG mode using high-viscosity crude oil. They found that the gas solubility in crude oil was enhanced due to the LSW, which enhances the mobility ratio between the displacing fluid and displaced fluid leading to improved oil recovery. The same trend has been observed in other experimental studies.[12−14]

Received: February 18, 2023
Revised: March 31, 2023

Table 1. Summary of Low-Salinity Polymer Flooding Experimental Studies

ref	rock type (reservoir)	clay content	formation brine (mg/L)	injected brine (mg/L)	polymer type/concentration	temperature	remarks
23	berea sandstone	clay content = 5 wt % kaolinite, illite, chlorite	33,793	3338	3330S HPAM 2500 ppm	85 °C	(1) low-salinity polymer resulted in 10% decrease in residual oil saturation. (2) maximum oil recovery was achieved with fewer pore volumes injected.
21	berea sandstone	clay content = 7.9 wt % kaolinite, illite, chlorite	36,318	3600	3630S HPAM 300−1000 ppm	22 °C	low polymer concentration of 300 ppm, LSP gave very high incremental oil recoveries between 10 and 17%.
22	carbonate	N/A	244,000	69,000	sulfonated polyacrylamide 2000−3000 ppm	N/A	(1) combined process also resulted in 6.5−9.9% additional oil recovery in comparison with the oil recovery expected from the individual process. (2) combined process required significantly lower polymer concentration.
24	berea and bentheimer sandstones	clay content = 0.7−6.5 wt % kaolinite	197,451	3360	HPAM 5000 ppm	60 °C	(1) low-salinity polymer flooding provided higher incremental oil recovery. (2) initial wetting state and clay content influenced the LSP performance.
25	outcrop sandstone	clay content = 9.9−11.6 wt % illite, chlorite	100,000	1000	3630S HPAM 1000 ppm	60 °C	(1) secondary LSP gave 2−4% incremental oil recovery. (2) tertiary LSP gave 22% incremental oil recovery.
26	sandstone	N/A	41,160	4112	HPAM 6035S 200−500 ppm	45 °C	(1) combination of smart waterflooding and polymer flooding resulted in increased oil recovery.
27	sandstone	clay content = 3 wt % illite, chlorite, kaolinite	6230	785	3430S HPAM 1400 ppm	58 °C	(1) polymer retention when using LSP was significantly lower than that in the other cases. (2) LSP has the potential to expand the application envelope of polymer flooding.
28	sandstone	clay content = 2 wt % bentonite	32,754	3,276−32,756	PAM 2000 ppm	70 °C	(1) LSP reduces adsorption of polymer on rock. (2) LSP can significantly improved oil recovery compared to the separate LSWF and polymer flooding.
29	sandpack	>99% silica	40,000−160,000	2000−6000	Flopaam 3630S HPAM 100, 200 ppm	ambient temperature	(1) polymer addition reduced the length of the mixing zone by up to 49% and delayed breakthrough times. (2) higher brine salinity reduces the efficiency of HPAM. (3) 200 ppm HPAM reduces dispersivity by 70%.

https://doi.org/10.1021/acs.energyfuels.3c00542
Energy Fuels XXXX, XXX, XXX−XXX

A low-salinity waterflooding and surfactant flooding hybrid makes use of the wettability alteration mechanism of LSWF and IFT reduction of surfactant flooding. Oil recovery improvement due to the combined effect of low-salinity water and surfactant flooding has been reported in coreflooding experiments by Alameri et al.[15] in oil-wet carbonate core samples. Jha et al.[16] observed that a combination of low-salinity waterflooding, surfactant, and an optimum concentration of nanoparticles resulted in a significant improvement of oil recovery compared to low-salinity surfactant flooding. Kumar et al.[17] evaluated the use of a novel nanofluid formulation (positively charged Ludox CL silica nanoparticle and anionic Aerosol-OT surfactant) in a low-salinity seawater base brine through spontaneous imbibition core tests. Their results showed that this nanofluid formulation led to the highest oil recovery from a Berea sandstone sample compared to the cases in which deionized water, LSW, pure silica nanoparticles, or pure surfactant (AOT) were used. This was attributed to the strong wettability alteration of the rock sample, significant IFT reduction and excellent stability of the nanofluid.

1.1. Low-Salinity Polymer Flooding. The focus of this work is modeling a combination of low-salinity waterflooding and polymer flooding. Polymer flooding is the injection of polymer-containing aqueous solution into the reservoir from an injector driving the oil into the producer. Addition of polymer to the injected water increases the viscosity of the displacing (injected) phase, which improves the sweeping process by resulting in a favorable mobility ratio.[18−20] Combining the low-salinity waterflooding with polymer flooding utilizes the advantage of the wettability alteration induced by LSWF and the improved mobility control resulting from polymer flooding.

Low-salinity polymer flooding (LSP) has been investigated experimentally in different studies. Kozaki et al.[21] found that at a low polymer concentration of 300 ppm, LSP gave very high incremental oil recoveries ranging between 10 and 17% in their coreflooding runs on the Berea sandstone cores. Shiran and Skuage[22] studied the possibility of combining low-salinity waterflooding and polymer flooding utilizing coreflooding in Berea sandstone samples. Results showed that injection of low-salinity polymer resulted in a 10% reduction in the residual oil saturation and that the maximum oil recovery was achieved with fewer pore volumes injected. In carbonate coreflooding, AlSofi et al.[23] found that the performance of the combined smart water/polymer flooding required significantly lower polymer concentration in comparison with high salinity polymer flooding. The combined process also resulted in 6.5−9.9% additional oil recovery in comparison with the oil recovery expected from the individual processes. Table 1 presents a summary of the published experimental studies conducted to investigate the performance of low-salinity polymer flooding.

1.2. Polymer Rheological Properties. The most widely used synthetic polymers are polyacrylamide (PAM) and hydrolyzed polyacrylamide (HPAM), while xanthan gum is the most popular natural polymer for EOR applications.[30] Hydrolyzed polyacrylamide (HPAM) is preferred in enhanced oil recovery mainly due to its good viscosity improvement properties. With several successful polymer flooding field applications reported in the literature, the common expectation of incremental oil recovery is between 15 and 20% over waterflooding.[31] However, the HPAM polymer tends to degrade at high temperatures and is sensitive to salinity.[30] For this reason, the combination of polymer flooding with low-salinity waterflooding helps to reduce the extent of polymer degradation. It was also found that polymer adsorption decreases with decreasing salinity. Polyacrylamide tends to strongly adsorb on the rock surface. Hence, the polymer is partially hydrolyzed to reduce this adsorption by converting some of the amide groups ($CONH_2$) to carboxyl groups ($COO-$) as shown below[32,33]

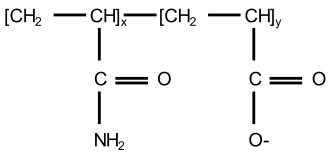

Polymer rheological properties and adsorption are strongly dependent on brine salinity. Luo et al.[34] suggested that the polymer viscosity is more sensitive to divalent cations such as Ca^{2+} and Mg^{2+} than monovalent cations i.e., Na^{+}. This is particularly important in polymer flooding and low-salinity polymer flooding, as the targeted dissolved solids for salinity reduction are mainly the divalent cations due to their higher effect on ionic strength and oil adhesion.[33,35−38] Temperature increase causes rapid thermal degradation of the HPAM polymer, reducing its viscosity.[39−41] As temperature increases, the activity of the polymer chain increases, and the friction between the molecules decreases causing the viscosity to decrease.[34] Hence, the inclusion of the temperature effect on the polymer's viscosity in modeling and simulation is important for the accurate prediction of polymer flooding performance.

To predict the viscosity of HPAM polymer solution, the power-law model (eq 1) can be used to describe its pseudoplastic behavior

$$\mu_p = K\dot{\gamma}^{(n-1)} \tag{1}$$

where μ_p is the viscosity of the polymer in cP, $\dot{\gamma}$ is the shear rate in s^{-1}, K is the flow consistency index, and n is the flow behavior index. The effect of polymer concentration and salinity on the polymer viscosity at zero shear rate, μ_p^0, can be described by the Flory−Huggins equation (eq 2)

$$\mu_p^0 = \mu_w(1 + (A_{p1}C_p + A_{p2}C_p^2 + A_{p3}C_p^3)C_{sep}^{Sp}) \tag{2}$$

where μ_w is the water viscosity, C_p is the polymer concentration, C_{sep} is the effective salinity of the polymer, and A_{p1}, A_{p2}, A_{p3}, and Sp are polymer-specific empirical constants. To calculate the viscosity of HPAM at temperature T based on a known viscosity $\mu_{p,ref}$ at a reference temperature T_{ref} is given as follows[34]

$$\mu_p = \mu_{p,ref}\exp\left[E_a\left(\frac{1}{T} - \frac{1}{T_{ref}}\right)\right] \tag{3}$$

where E_a is an empirical constant. The ζ potential of a polymer is also reliant on the concentration, salinity, and temperature of the polymer among other factors. In this work, we propose the use of the ζ potential to evaluate the viscosity of the HPAM polymer.

1.2.1. Polymer−Brine−Rock Interactions. The presence of ($-COO-$) in the polymer solution reduces adsorption and increases polymer viscosity due to repulsion between the similarly charged ($-COO-$) groups which causes the polymer

https://doi.org/10.1021/acs.energyfuels.3c00542
Energy Fuels XXXX, XXX, XXX−XXX

chain to expand. However, hydrolysis makes the polymer chain more sensitive to the ionic environment as more (−COO−) surface groups are produced, and they react easily with the cations in the aqueous solution. These reactions with the cations result in the screening of the charge at the end of polymer chains resulting in a coil shrinking effect as well as increasing adsorption on the clay surface, especially in the presence of multivalent cations.[42] Higher temperatures also result in less polymer being adsorbed on solid surfaces. This is a result of the enhanced electrostatic repulsion as the negative charge on both the rock surface and polymer chains increases as the temperature rises.

Polymer adsorption on the rock surface is also dependent on the type of rock. Carbonate rocks are known to have a positive surface charge under normal reservoir conditions, which results in a higher attraction between the negatively charged −COO− and the positively charged carbonate surface. Polymer adsorption on the sandstone surface is dependent on the clay content and sandstone mineralogy. Sandstone rocks with higher clay content have a higher number of surface site densities available for cations to adsorb on, incurring the higher negative surface charge screening. Hence, higher clay content leads to a higher attraction between the polymer chains and sandstone surfaces resulting in more polymer adsorption.[43]

The polymer rheological properties are governed by the polymer−brine interface interactions, hence, understanding and quantifying these interactions should be of great importance in any modeling approach. This allows for the adsorption mechanism and forces acting between the polymer chains and the rock surfaces to be evaluated mechanistically. Surface complexation modeling utilizes the thermodynamic equilibria theory to describe the adsorption of ions from an aqueous phase to the surface groups of a solid surface. Various surface complexation models are present and differ in their description of the electrical interfacial layer. In this work, we utilize triple-layer surface complexation modeling which describes the electrical interfacial layer as three layers, the inner and outer Helmholtz layers and the diffuse layer. The inner and outer Helmholtz layers together are known as the stern layer. A depiction of a triple-layer model of the negatively charged solid surface is presented in Figure 1.

A limited number of surface complexation models were developed to understand the polymer−brine interface interactions. Three surface complexation models were developed by Katz and Hayes[44] to describe the adsorption of the cobalt polymer on solid surface hydroxyl groups, these are the surface solid solution model, surface polymer model, and continuum model. Modeling results were compared with experimental spectroscopic data for a wide range of surface coverage. They found that the continuum model, which allows for the formation of surface polymers and precipitants, represents the most logical option to simulate polymer adsorption compared to the surface solid solution model and surface polymer model. However, their work is based on the assumption that the polymer is a sorbed species rather than a sorbing surface itself. Moreover, the adsorption of the cobalt polymer on the solid surface was described by geochemical and surface complexation reactions, instead of including the repulsive and attractive interaction forces between the polymer−brine and rock−brine interfaces.

Saha and Streat[45] proposed a surface complexation model to describe the polymer−brine interfaces of the macronet

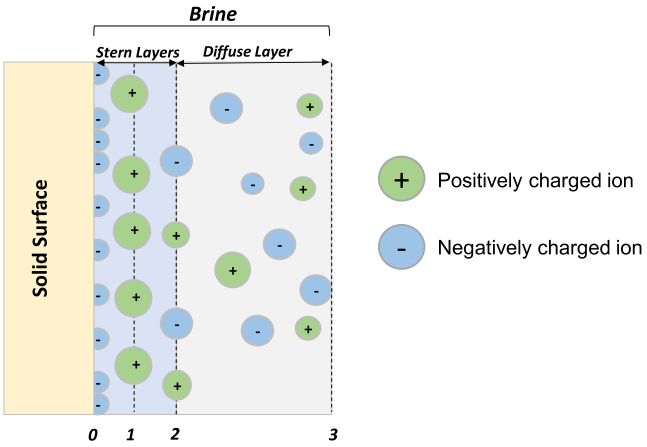

Figure 1. Depiction of a triple-layer surface complexation model of a negatively charged surface and different ions present in the electric layer. The different sizes of the circles reflect the different ion sizes present in the system where the larger oppositely charged ions are present on the 1-plane closer to the surface.

polymer, MN-600, and acrylic resin, C-104E. Their model described the deprotonated carboxyl groups (−COO−) as the sorbing surface groups on the polymer's surfaces and considered the sorption of the H^+, Cu^{2+}, Zn^{2+}, and Ni^{2+} as the potential determining ions (PDIs) on them. Their surface complexation modeling results showed good agreement with experimental results, especially for the macronet polymer. However, their work was limited to MN-600 and C-104E polymers and the adsorption of only H^+, Cu^{2+}, Zn^{2+}, and Ni^{2+} on the polymer's surface groups. Hence, their surface complexation model cannot be applied in the case of using the HPAM polymer in sandstone reservoirs where the ionic composition of the formation brines significantly differs from the modeled PDIs.

This work focuses on investigating the interfacial chemical interactions within a polymer−brine−sandstone rock system which dictates HPAM polymer's viscosity and adsorption on the sandstone surface. To achieve this objective, a novel approach is presented, which includes the development of a new triple-layer surface complexation model (TLM) to describe the HPAM polymer−brine interface. The proposed model overcomes the shortcomings of previously developed models by describing (i) the polymer as a sorbing surface rather than a sorbed species and specifically defines the carboxylic groups as the sorbing species on the polymer's surface, (ii) the adsorption of various potential determining ions to the polymer's −COOH groups including H^+, Na^+, Ca^{2+}, and Mg^{2+}, which are the most expected cations in the formation water of a typical sandstone reservoir. This model is based on the assumption that the polymer−brine interface can be depicted as a triple-layer model. Moreover, the literature review revealed that there is a lack of comprehensive surface complexation models to account for the HPAM polymer−brine−sandstone interactions. Hence, polymer−brine the proposed TLM will be analyzed with our previously developed sandstone−brine TLM[46] to gain insights into the relationship between the polymer adsorption to the rock surface and the interactions between the polymer and rock surfaces. Additionally, polymer viscosity and ζ potential are dictated by similar parameters such as brine ionic composition, temperature, and polymer concentration, however, the relationship between the viscosity and ζ potential is not well defined in published

https://doi.org/10.1021/acs.energyfuels.3c00542
Energy Fuels XXXX, XXX, XXX−XXX

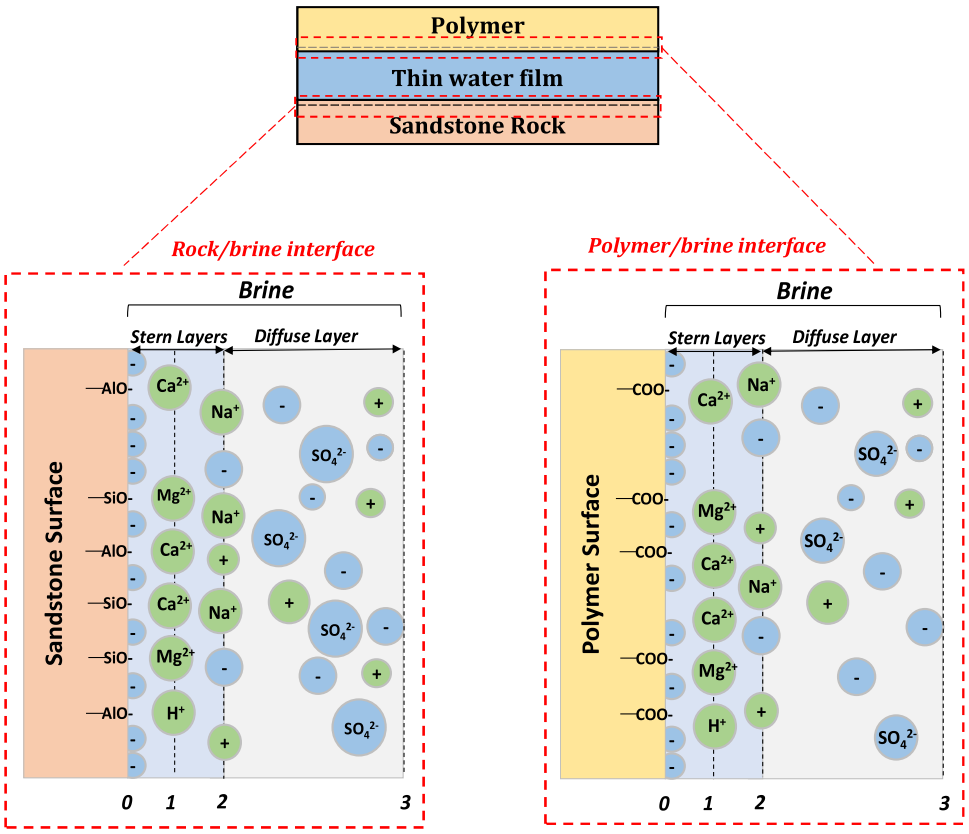

Figure 2. Representation of (top panel) polymer−brine-rock interface, (bottom panel) rock−brine, and polymer−brine triple-layer models. Reproduced with permission from.[46] Copyright 2022. Elsevier.

studies. This gap is also being exploited in this work thereby establishing the relationship between the polymer's viscosity and ζ potential. Both HPAM polymer viscosity and adsorption are of particular interest during polymer flooding processes. This work presents a novel approach to investigating the interactions occurring within the polymer−brine−rock interfaces during polymer flooding and low-salinity polymer flooding in sandstone reservoirs.

2. METHODOLOGY

A triple-layer surface complexation model (TLM) is developed to describe the interactions at the HPAM polymer−brine and brine−rock interfaces as depicted in Figure 2. The polymer−brine interface model shown in Figure 2 and adopted in this work is considered a simplification of the real-life case of polymer−brine which takes the shape of coiled spring. This is more complex than the flat plane adopted here and consequently the model shall only provide an approximation of the expected charging behavior at polymer−brine interface. The proposed model was then coupled with the extended Derjaguin, Landau, Verwey, and Overbeek (DLVO) theory to analyze polymer rheology as a function of the polymer solution interfacial properties.

2.1. HPAM Polymer−Brine Triple-Layer Surface Complexation Model. A TLM was developed in this work using the charge distribution multisite surface complexation model (CD-MUSIC) module in the state-of-the-art geochemical code PHREEQC version 3. Triple-layer surface complexation models allow for the modeling of both inner and outer sphere complexes compared to double-layer models. TLMs also enable the placement of adsorption planes at different varying distances depending on the adsorbed species. For these reasons, TLMs are more robust than double-layer models in modeling surface complexation behavior.[47,48] To develop a polymer−brine TLM, the following parameters are defined: polymer surface complexation reactions and equilibrium constants, capacitances of the inner and outer Helmholtz layers, charge distribution, polymer surface group site density, and polymer-specific surface area. The carboxylate (−COOH) group is proposed as the surface-acting group on the polymer surface in this model. It is assumed that the surface site density of the −COOH group is a function of polymer concentration and polymer hydrolysis. Hence, the surface site density can be calculated as follows

$$N_{\text{spolymer}}\left(\frac{\text{site}}{\text{nm}^2}\right) = \text{hydrolysis (\%)} \times \text{polymer concentratio}$$
$$\text{n(ppm)} \times N_0 \quad (4)$$

where N_0 is a polymer-specific parameter that we determined it to be 0.002 in our current work by fitting the predicted ζ potential value to the experimental values adopted from the literature. Equation 4 is proposed to estimate the polymer's surface site density and can be physically explained by the fact that the number of available sites are expected to be higher with higher polymer concentration. The percentage of hydrolyzed polymer chains i.e., hydrolysis, dictate the percentage of polymer chains that were hydrolyzed to convert amide groups ($CONH_2$) to carboxyl groups (COO−). Hence, the higher the hydrolysis the higher the number of adsorption sites. And because polymers have different chemical structures, the polymer-specific parameter, N_0, was introduced. The

https://doi.org/10.1021/acs.energyfuels.3c00542
Energy Fuels XXXX, XXX, XXX−XXX

Table 2. Association/Disassociation Constants, Charge Distribution, and Capacitance Values Used in the Polymer−Brine Model

surface complexation reaction	log K @ 25 °C	charge distribution			C_1 (F/m^2)	C_2 (F/m^2)
		0-plane	1-plane	2-plane		
polymer − COOH ↔ −COO$^-$ + H$^+$	−4.7	−1	0	0	2.57	2.57
polymer − COOH + Ca^{2+} ↔ −COOCa$^+$ + H$^+$	−3.7	−1	+2	0	3.54	2.57
polymer − COOH + Mg^{2+} ↔ −COOMg$^+$ + H$^+$	−3.7	−1	+2	0	4.92	2.57
polymer − COOH + Na$^+$ ↔ −COONa + H$^+$	−4	−1	+0.5	+0.5	2.57	2.57
polymer − COOH + SO_4^{2-} ↔ −COO$^-$ + HSO_4^-	−3.3	−1	0	0	2.57	2.57

Table 3. Quartz−Brine TLM Reactions, Charge Distribution, and Capacitance Values Used in the Model[46]

surface complexation reaction	log K @ 25 °C	enthalpy (kJ/mol)	charge distribution			C_1 (F/m^2)	C_2 (F/m^2)
			0-plane	1-plane	2-plane		
>AlOH + H$^+$ ↔ >$AlOH_2^+$	0.8	−5	+1	0	0	2.57	2.57
>AlOH ↔ >AlO − +H$^+$	−7.5	−40	−1	0	0	2.57	2.57
>AlOH + Na$^+$ ↔ >AlONa + H$^+$	−4.5	−60	−1	+0.5	+0.5	2.57	2.57
>AlOH + Ca^{2+} ↔ >AlOCa$^+$ + H$^+$	−3.5	−50	−1	+2	0	3.54	2.57
>AlOH + Mg^{2+} ↔ >AlOMg$^+$ + H$^+$	−3.5	−50	−1	+2	0	4.92	2.57
>AlOH + SO_4^{2-} ↔ >AlO$^-$ + HSO_4^-	−1.5		−1	0	0	2.57	2.57
>SiOH ↔ >SiO$^-$ + H$^+$	−6.5	−40	−1	0	0	2.57	2.57
>SiOH + Na$^+$ ↔ >SiONa + H$^+$	−2	−60	−1	+0.5	+0.5	2.57	2.57
>SiOH + Ca^{2+} ↔ >SiOCa$^+$ + H$^+$	−2.5	−50	−1	+2	0	3.54	2.57
>SiOH + Mg^{2+} ↔ >SiOMg$^+$ + H$^+$	−2.8	−50	−1	+2	0	4.92	2.57
>SiOH + SO_4^{2-} ↔ >SiO$^-$ + HSO_4^-	−1.5		−1	0	0	2.57	2.57

polymer-specific surface area was fixed at 1 g/m^2 for simplification and due to its negligible influence when the cation affinities for adsorption are relatively high.[49] The potential determining ions (PDIs) adopted in the developed polymer−brine model are H$^+$, Na$^+$, Ca^{2+}, Mg^{2+}, and SO_4^{2-}. The association and dissociation equilibrium constants for the PDIs, H$^+$, Ca^{2+}, and Mg^{2+}, were optimized by comparing the ζ potential predicted using the developed polymer−brine TLM with experimental ζ potential values from Al-Busaidi.[50] While the association constants for Na$^+$ and SO_4^{2-} were adopted from Saeed et al.[51] because the carboxylic surface group is also active on the oil surface. Hence, the reactions, capacitance values, and charge distribution for the developed polymer−brine TLM in this work are listed in Table 2. The capacitance values depend on the adsorbed ion size, more details on the capacitance calculations are reported by Saeed et al.[51]

After validating the developed polymer−brine TLM by comparing the model-predicted ζ potential with the experimental ζ potential values from Al-Busaidi,[50] experimentally measured viscosity values adopted from the published literature were analyzed using the modeled ζ potential. Because both polymer viscosity and ζ potential are dictated by the electrical surface properties and interactions. Furthermore, by utilizing regression analysis, correlations between the polymer viscosity and ζ potential, at varying salinities, polymer concentrations, and temperatures were developed. The details of the correlation development and their performance against experimental data are further detailed in Section 2.4.

2.2. Sandstone Rock−Brine Triple-Layer Surface Complexation Model. The sandstone−brine TLM utilized in this work is adopted from Saeed et al.[46] where the developed model was validated against various experimental datasets under varying conditions and for different types of sandstone rocks. The adopted sandstone−brine model was run using the CD-MUSIC module in PHREEQC. The sandstone surface groups, > AlOH and > SiOH, go through various protonation/deprotonation and association/dissociation reactions with the PDIs present in the brine. The sandstone rock−brine surface complexation reactions, their equilibrium constants, capacitance values, and charge distribution adopted in the model are summarized in Table 3. Further details of the adopted sandstone−brine TLM can be found in Saeed et al.[46]

2.3. Disjoining Pressure, Interaction Potential Energy, and Maximum Energy Barrier. The disjoining pressure and interaction potential of the polymer−brine−quartz system can be calculated as the summation of three components according to the DLVO theory. These three components are the van der Waals force, the structural force, and the electrical double-layer force. Calculating the electrical double-layer force requires the knowledge of ζ potential values at both polymer−brine and sandstone−brine interfaces. In this work, we import these required ζ potential values from the proposed polymer−brine and sandstone−brine TLMs presented in the previous sections. To calculate the electrical double-layer forces between two charged interfaces several methods are present to approximate the solution including constant potential, constant charge, and charge regulation.[52] In

https://doi.org/10.1021/acs.energyfuels.3c00542
Energy Fuels XXXX, XXX, XXX−XXX

this work, we use the constant potential solution, which is written as follows[53]

$$\Pi_{\text{electric}}(h) = n_b k_b T\left(\frac{2\psi_{r1}\psi_{r2}\cos h(\kappa h) - \psi_{r1}^{\ 2} - \psi_{r2}^{\ 2}}{[\sinh(\kappa h)]^2}\right) \quad (5)$$

where n_b is the ion density in the bulk solution, k_b is the Boltzmann constant (1.38×10^{-23}J/K), ψ_{r1} and ψ_{r2} are the reduced surface potentials for the rock−brine and oil−brine interfaces, respectively, and κ is the Debye−Hückel reciprocal length. The van der Waals forces can be calculated using the following equation[54]

$$\Pi_{\text{vdW}}(h) = -\frac{A\left(15.96\left(\frac{h}{\lambda_{lw}}\right) + 2\right)}{12\pi h^3\left(1 + 5.32\left(\frac{h}{\lambda_{lw}}\right)\right)^2} \quad (6)$$

where, λ_{lw} is the London wavelength and can be assumed to be 100 nm,[54] h is the distance between the two plates and A is the Hamaker constant. The structural forces between two parallel plates can be calculated by

$$\Pi_{\text{structural}}(h) = A_s e^{-h/h_s} \quad (7)$$

where A_s is a coefficient, assumed to be 1.5×10^{10} Pa[55] and h_s is the characteristic length, assumed to be 0.05 nm.[55] The specific interaction potential energy can be calculated using the following equation[55]

$$\omega = \int_h^{h_{eq}} (\Pi - \Pi_{eq}) \cdot dh \quad (8)$$

where h_{eq} and Π_{eq} are the separation distance and disjoining pressure at equilibrium conditions, respectively. The maximum energy barrier (MEB) is defined as the maximum of the specific interaction potential energy curve, which is an indicator of the stability of the colloidal system.[55] The higher the MEB, the higher will be the stability of the system. In this work, we propose the use of the maximum energy barrier as an indicator of the polymer adsorption to the rock surface. For this application, it was observed that the MEB for an HPAM polymer−brine−quartz system occurs at film thicknesses between 0.5 and 1.5 nm, hence, the MEB for all the evaluated cases is calculated within this range.

2.4. Correlating the HPAM Polymer Viscosity with ζ Potential. The experimental dataset of Flopaam 3630s HPAM as reported by Lee[35] was employed to find a correlation between the measured viscosity and model-predicted ζ potential under different conditions. The polymer rheological properties considered are bulk properties and should be considered within that context of bulk flow. The workflow followed to develop the correlation is described in Figure 3. The workflow starts by extracting the power-law coefficients from the experimental dataset of Lee.[35] The next step was to predict the ζ potential at the polymer−brine interface using the developed TLM under the experimental conditions. The extracted power-law coefficients and consequently viscosity is then correlated with the predicted ζ potential values through non-linear regression. New correlations are then developed to predict the power-law coefficients and solution viscosity as a function of ζ potential, which in turn is a variable in terms of salinity, polymer concentration, and temperature. The new correlations were then used to calculate the new power-law coefficients at specific conditions. The viscosity curves

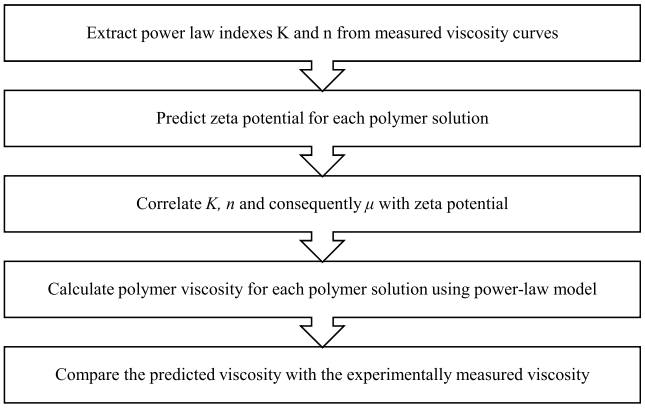

Figure 3. Workflow for correlating polymer viscosity with ζ potential.

predicted using the new power-law coefficients as a function of shear rate are then compared with the experimental results reported by Lee.[35] Furthermore, the developed correlation was used to perform a sensitivity analysis of HPAM polymer viscosity to salinity, temperature, and polymer concentration.

2.5. Correlating the HPAM Polymer Adsorption with the Maximum Energy Barrier. The HPAM polymer adsorption data reported by Page et al.[56] was analyzed with respect to the calculated maximum energy barrier. The process of analyzing the HPAM polymer adsorption as a function of the MEB is described in Figure 4. The process starts by

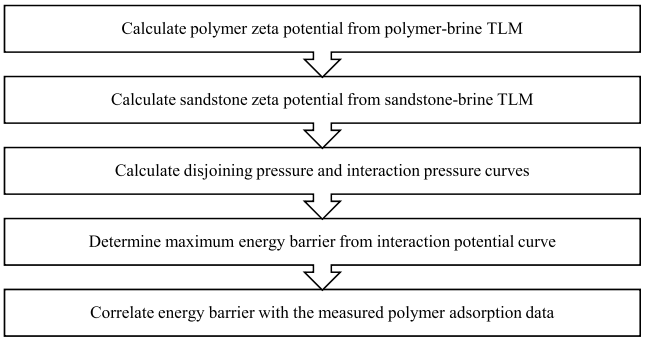

Figure 4. Workflow for correlating polymer adsorption with the energy barrier.

predicting the ζ potentials at both polymer−brine and sandstone−brine interfaces utilizing the proposed polymer−brine and sandstone−brine triple-layer models. The DLVO theory was then used to calculate the disjoining pressure and interaction potential. Consequently, the MEB was determined from the interaction potential curve. Finally, the calculated MEB was correlated with the HPAM polymer adsorption data reported by Page et al.[56] The adsorption data adopted from Page et al.[56] are measured from bulk adsorption tests and not from porous media flow tests. Hence, the developed correlations only reflect the electrochemical adsorption phenomena rather than the mechanical retention, which would also play a part in polymer retention during fluid flow in porous media.

3. RESULTS AND DISCUSSION

In this section, the validation of the developed polymer−brine TLM and the correlation developed between the polymer's viscosity and ζ potential is discussed and validated against the

https://doi.org/10.1021/acs.energyfuels.3c00542
Energy Fuels XXXX, XXX, XXX−XXX

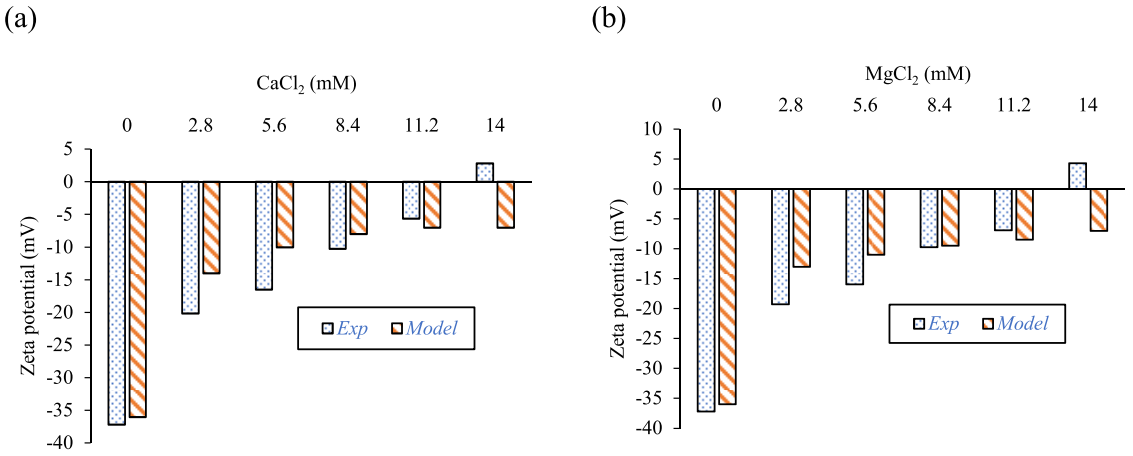

Figure 5. Experimental and modeled ζ potential for Flopaam 3630s in (a) $CaCl_2$ brine and (b) $MgCl_2$ brine (experimental results from Al-Busaidi[50]).

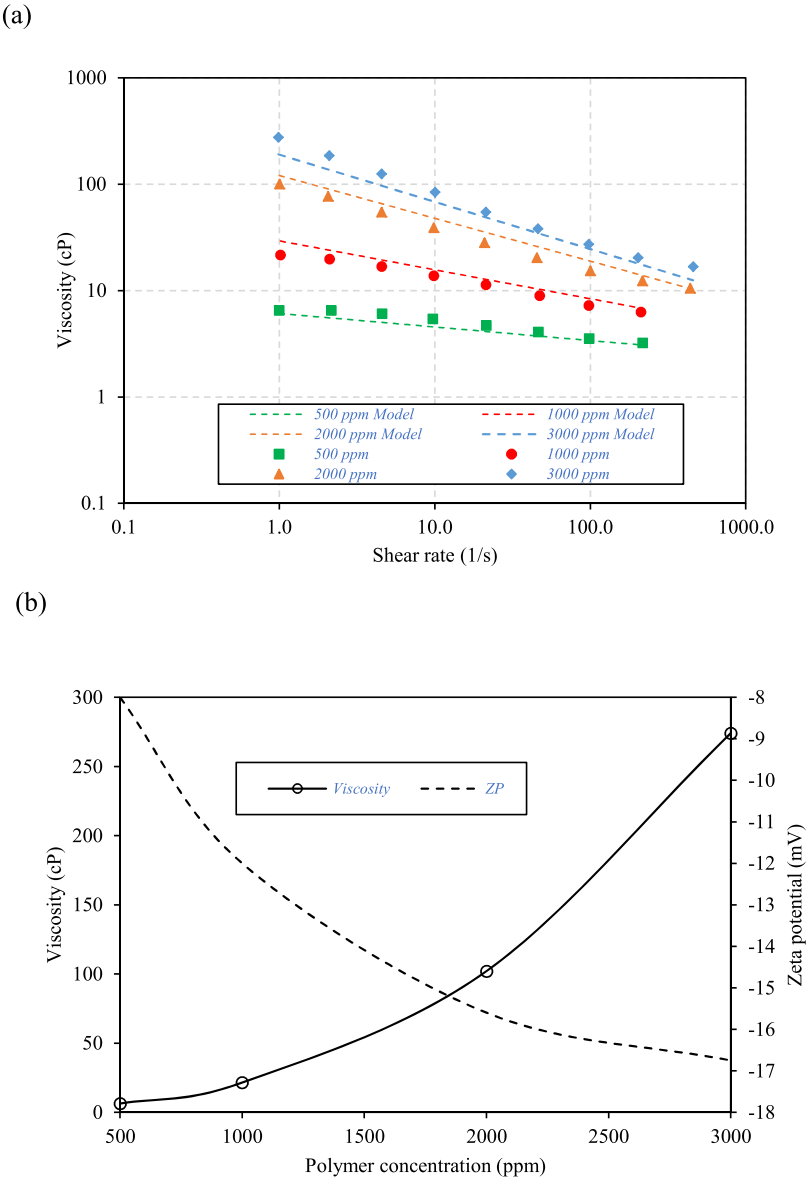

Figure 6. (a) Comparison between measured and correlation-predicted viscosity curves at various polymer concentrations at 1% NaCl salinity and 25 °C (experimental data from[35]). (b) Effect of polymer concentration on viscosity and ζ potential.

https://doi.org/10.1021/acs.energyfuels.3c00542
Energy Fuels XXXX, XXX, XXX−XXX

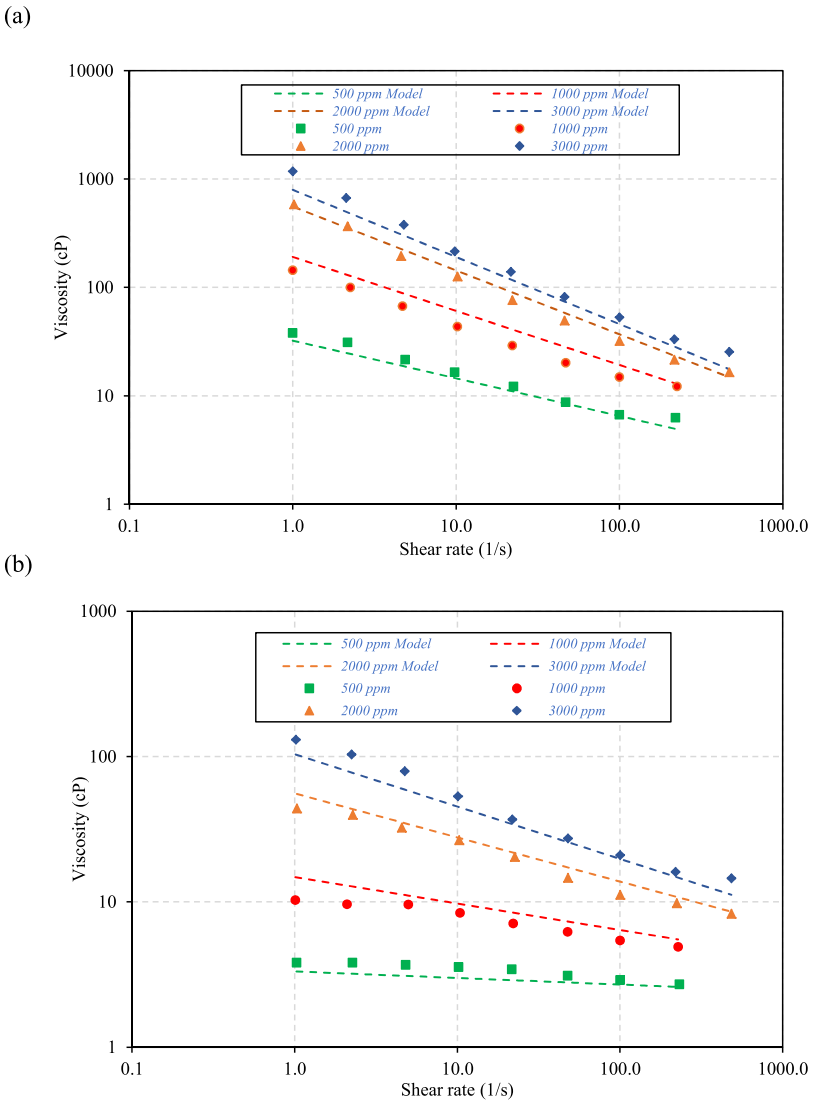

Figure 7. Comparison between measured and correlation-predicted viscosity curves at various polymer concentrations at 25°C (a) 4 wt % NaCl salinity and (b) 0.1 wt % NaCl salinity (experimental data from[35]).

experimental dataset reported by Lee.[35] Results of the sensitivity analysis of HPAM polymer viscosity to salinity, temperature, and polymer concentration are discussed. Later, the results of correlating HPAM's polymer adsorption data as a function of the MEB are reported.

3.1. ζ Potential Validation. The polymer−brine ζ potential predicted from the developed TLM was validated against Flopaam 3630s ζ potential data from Al-Busaidi.[50] A comparison between the ζ potential predicted from the TLM against the experimentally measured ζ potential values in pure brine and $MgCl_2$ and $CaCl_2$ brines is shown in Figure 5. The brine salinity ranged from 0 to 14 mM and ζ potential values were predicted at 25 °C. The model was able to replicate the experimental trend of ζ potential at varying salinities where the increase in salinity resulted in an increase of the ζ potential value. The modeling results showed a 0.92 correlation coefficient between the model ζ potential and experimental ζ potential. There is a lack of experimental ζ potential data for further validating the developed TLM and depending on the availability of this data, the model can be further validated and calibrated.

3.2. ζ Potential Predicted Viscosity. The approach described in Section 2.4 was used to correlate the polymer solution viscosity and ζ potential as a function of polymer concentration between 500 and 3000 ppm in 1% NaCl electrolyte at 25 °C. Regression analysis between the experimentally measured viscosity, μ, and model-predicted ζ potential, ζ, revealed the following correlation

$$\mu = (0.2627e^{-0.393\zeta}) \times \gamma^{(0.0362\zeta+0.1624)},\ R^2 = 0.995 \quad (9)$$

similarly, the correlation at 0.1% NaCl was

$$\mu = (0.0261e^{-0.178\zeta}) \times \gamma^{(0.0151\zeta+0.2563)},\ R^2 = 0.982 \quad (10)$$

and at 4% NaCl

$$\mu = (0.4e^{-1.411\zeta}) \times \gamma^{(0.1292\zeta+0.487)},\ R^2 = 0.961 \quad (11)$$

To validate the presented empirical correlation at 1% NaCl (eq 9), the experimentally measured viscosity values were compared with the viscosity values predicted from the correlation. The Flopaam 3630s database presented by Lee[35] was used in the validation process. Figure 6a shows the comparison between the measured and modeled viscosity

https://doi.org/10.1021/acs.energyfuels.3c00542
Energy Fuels XXXX, XXX, XXX−XXX

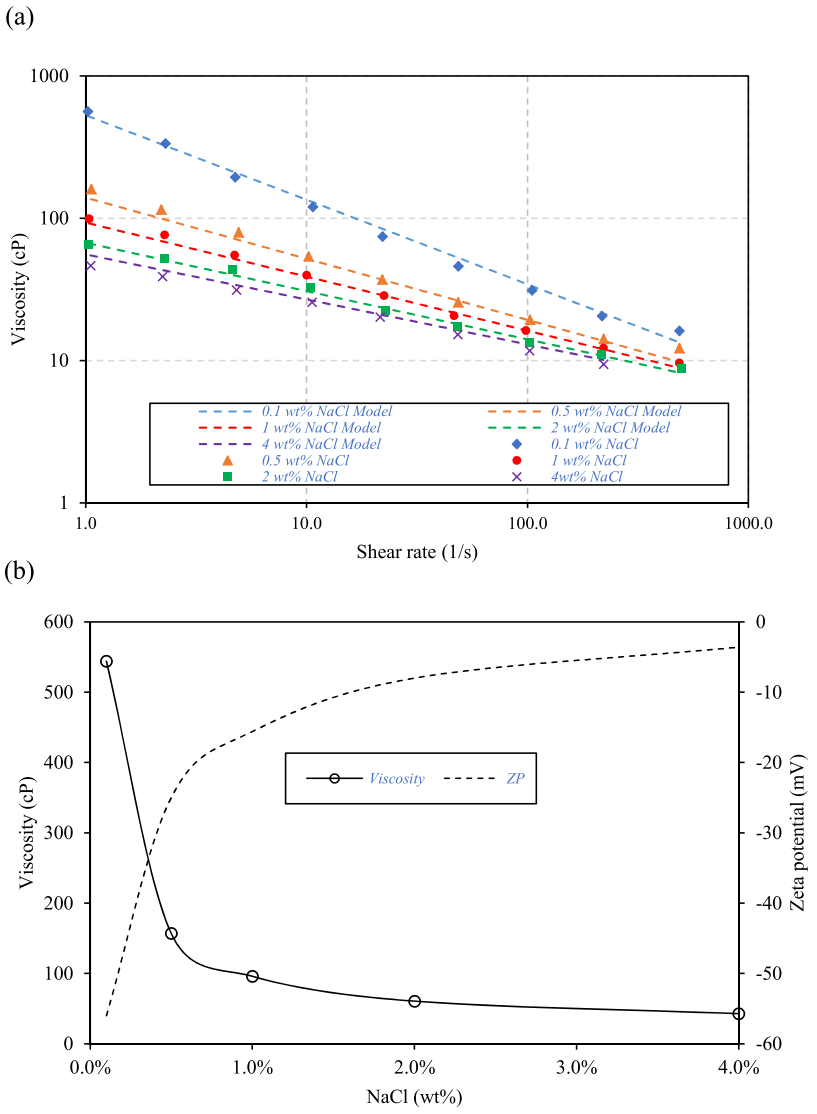

Figure 8. (a) Comparison between measured and correlation-predicted viscosity curves at various salinities at 2000 ppm polymer concentration and 25 °C (experimental data from[35]). (b) Effect of salinity on viscosity and ζ potential.

curves against shear rate for various polymer concentrations between 500 and 3000 ppm in 1% NaCl electrolyte at 25 °C. Results show small discrepancies at 3000 ppm polymer concentration, however, the rest of the modeling results at lower concentrations are satisfactory compared to the measured data. Figure 6b exhibits how the polymer concentration affects both the measured viscosity and TLM predicted ζ potential values. It demonstrates that an increase in the polymer concentration leads to higher polymer viscosity and higher negative ζ potential magnitudes The increase in the polymer concentration means a higher number of −COOH surface sites, which in turn deprotonate to give the negatively charged −COO− leading to a more negative polymer surface charge and ζ potential. This increase in the negative charge at the polymer chains causes repulsion between the polymer chains making them stretch, enhancing the polymer solution viscosity. Similarly, the correlations (eqs 10 and 11) were then used to predict the viscosity of the polymer at concentrations between 500 and 3000 ppm at both 0.1 and 4 wt % NaCl solutions and compare them with the measured values.[35] The comparison is depicted in Figure 7 and it shows that the proposed correlations give accurate predictions for the polymer viscosity. However, in the case of NaCl salinities of 0.1 wt % and 4% at a higher shear rate, the predicted viscosity shows contrast to the measured viscosity values. This is because the HPAM polymer exhibits shear thickening behavior at higher shear rates and the power-law model does not accurately capture such behavior.[35] This shear thickening behavior may also be attributed to instrument inertia effects (delays or inaccuracies in measuring changes in viscosity at high shear rates) and secondary flow effects (the formation of secondary flow patterns in the fluid, which can cause local variations in the shear rate). Both phenomena may contribute to the shear thickening behavior at higher shear rates.[57]

A correlation (eq 12) between the viscosity and ζ potential was developed as a function of salinity between 0.1 and 4 wt % NaCl at 25 °C at a fixed 2000 ppm polymer concentration

$$\mu = (47.725e^{-0.043\zeta}) \times \gamma^{(0.0053\zeta - 0.207)}, \quad R^2 = 0.996 \qquad (12)$$

Figure 8a presents a comparison between the measured and modeled viscosity values for various shear rates. This comparison demonstrates the model's ability to capture the effect of varying concentrations of NaCl on the polymer's

https://doi.org/10.1021/acs.energyfuels.3c00542
Energy Fuels XXXX, XXX, XXX−XXX

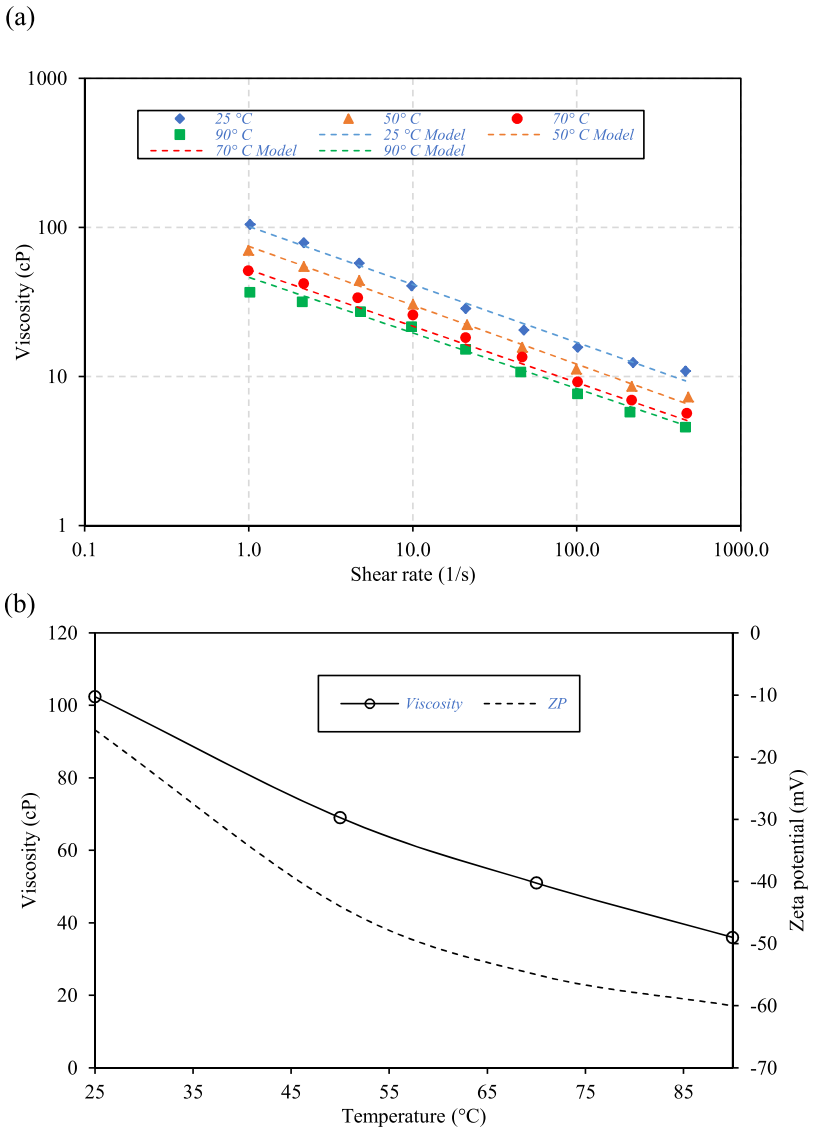

Figure 9. (a) Comparison between measured and correlation-predicted viscosity curves at various temperatures at 2000 ppm polymer concentration and 1 wt % NaCl salinity (experimental data from[35]). (b) Effect of temperature on viscosity and ζ potential.

viscosity. The model-predicted viscosity values were in agreement with the experimentally measured viscosities. In Figure 8b the effect of NaCl salinity on both the polymer's viscosity and ζ potential is presented. The decrease in viscosity and decrease in the negative ζ potential magnitudes with the increase in the salinity can be explained by the increased concentration of the monovalent Na^+ ions in the electrolyte. This increase in the positively charged sodium ions results in higher screening to the polymer surface's negative charge, which in turn leads to less repulsion between the polymer chains causing them to coil, hence decreasing the viscosity exhibited by the polymer. The enhanced negative charge screening is also reflected on the ζ potential as its magnitude becomes less negative which can be seen in Figure 8b. Therefore, the increase in salinity decreases the viscosity and increases the ζ potential value.

Another correlation (eq 13) was developed between the viscosity and ζ potential as a function of temperature between 25 and 90 °C using 2000 ppm concentration in 1 wt % NaCl electrolyte

$$\mu = (-0.0171\zeta^2 - 0.2608\zeta + 101.58)^* \gamma^{(3\zeta^2/10^5 + 0.0021\zeta + 0.6361)},\ R^2 = 0.985 \quad (13)$$

Figure 9a presents both the measured and model-predicted viscosity values using 2000 ppm concentration in 1 wt % NaCl electrolyte. Results show that the correlation viscosity was in satisfactory agreement with the experimentally measured values. Some discrepancies do exist at some data points between the measured and model value, however, overall, the correlation gives viscosity values within proximity to the measured data at high temperatures. This suggests that the empirical correlation presented in eq 13 can be used to capture the polymer's viscosity behavior at 2000 ppm concentration and 1 wt % NaCl electrolyte. Figure 9b, exhibits the impact of temperature on viscosity and ζ potential. It is apparent from two curves that increasing the temperature decreases the viscosity and increases the negative ζ potential magnitudes, which is a result of the degradation the polymer solution goes through the temperature increases leading to lower viscosities.

https://doi.org/10.1021/acs.energyfuels.3c00542
Energy Fuels XXXX, XXX, XXX−XXX

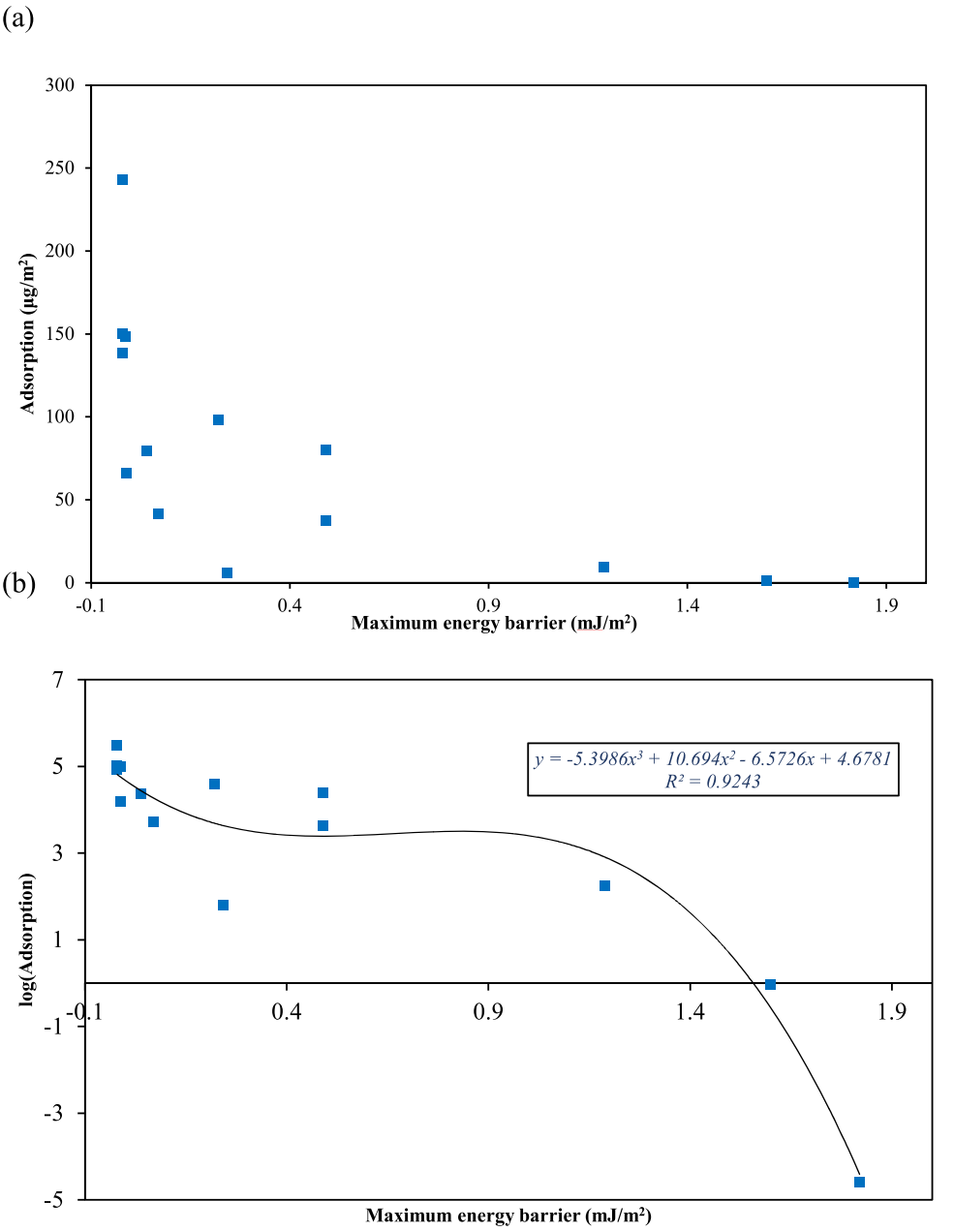

Figure 10. Measured polymer adsorption data (from Page et al.[56]) against the calculated maximum energy barrier on the (a) normal scale and (b) logarithmic *y*-axis scale.

While the increase in temperature increases the value of the ζ potential at the polymer−brine interface as a result of the enhanced deprotonation of the (−COOH) to give the negatively charged (−COO−) surface groups.

3.3. Correlation between Adsorption and Maximum Energy Barrier. A comparison between the maximum energy barrier and the experimental adsorption data is presented in Figure 10a where it can be seen that as the energy barrier decreases, the polymer adsorption increases. The polymer adsorption is at its highest value of 243 $\mu g/m^2$ at the lowest MEB value of −0.02 mJ/m^2. At MEB values higher than 0.5 mJ/m^2, the adsorption drops significantly to a range of 0−10 $\mu g/m^2$. This can be explained by the fact that the MEB represents the stability of the system. As the MEB increases, higher system stability is encountered leading to less attraction between the polymer chains and the rock surface. Hence, the conditions that promote higher MEB values lead to less polymer adsorption as well. In Figure 10b, logarithmic values of adsorption, c_{ad}, was plotted against the MEB where the polynomial correlation of the third-order in eq 12 fits the data presented with a 0.9243 R^2 value.

$$\log(c_{ad}) = -5.3986\omega_{max}{}^3 + 10.69\omega_{max}{}^2 - 6.573\,\omega_{max} + 4.6781 \quad (14)$$

where ω_{max} is the maximum energy barrier. This finding indicates that the proposed polymer−brine TLM can be used with the developed sandstone−brine TLM and the calculated energy barriers to predict the polymer adsorption expected at certain reservoir conditions and properties. The correlation presented above is applicable for a specific HPAM polymer with a specific concentration. The current correlation can be

https://doi.org/10.1021/acs.energyfuels.3c00542
Energy Fuels XXXX, XXX, XXX−XXX

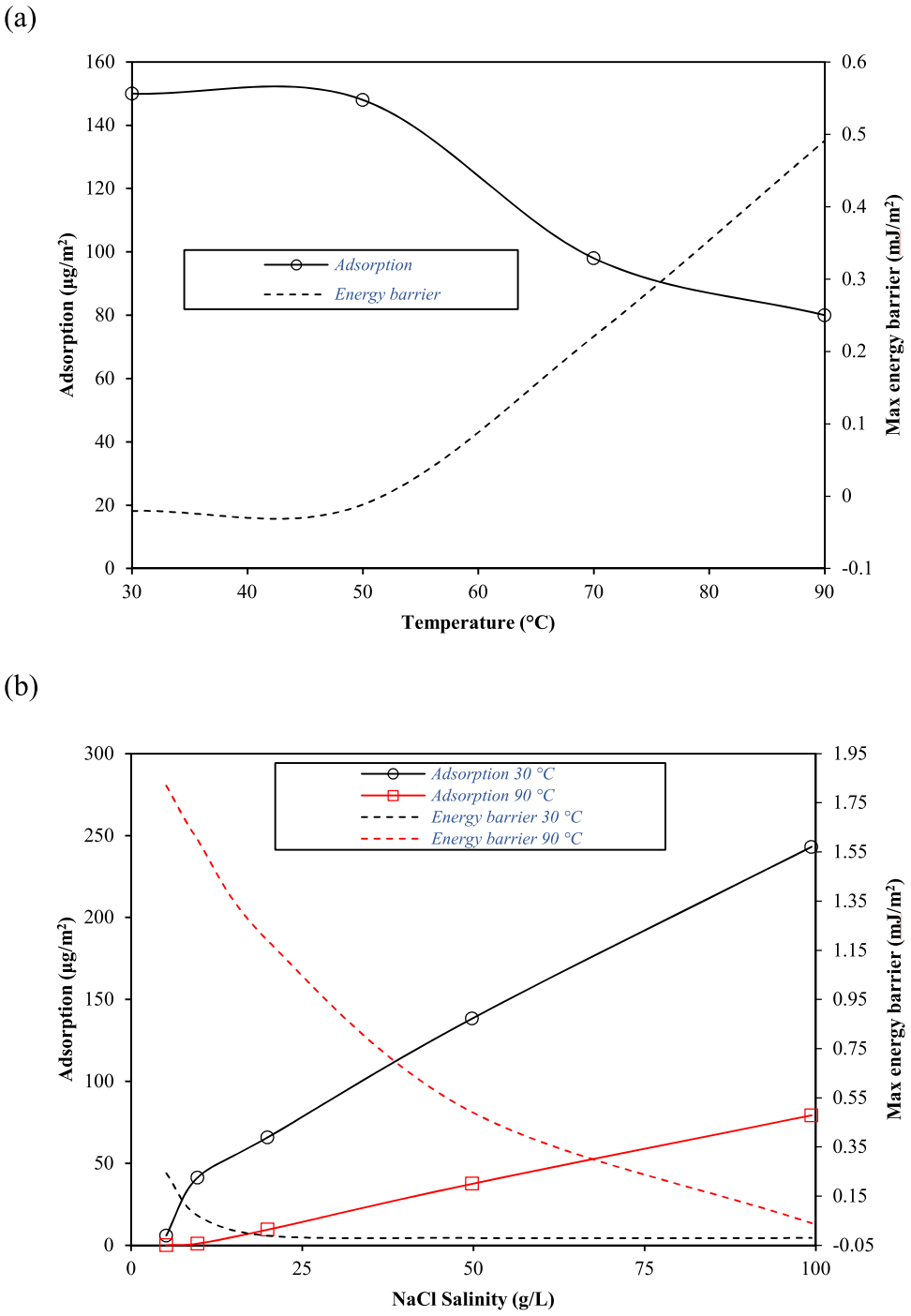

Figure 11. (a) Effect of temperature on the adsorption and energy barrier, (b) effect of salinity on the adsorption and energy barrier at 30 and 90 °C (adsorption data from Page et al.[56]).

modified to include the polymer concentration as a variable if more experimental data become available.

To understand the relationship between polymer adsorption as measured by Page et al.[56] and the MEB, the effects of temperature and salinity were investigated. Figure 11a presents the effect of altering the temperature between 30 and 90 °C on both adsorption and energy barrier. The plotted curves show that an increase in the temperature results in a higher energy barrier and lower polymer adsorption. This may be explained by the enhancement in the protonation of the polymer and sandstone surface groups to produce the negatively charged −COO− groups leading to higher repulsion between the polymer chains and the rock surface. This higher repulsion creates a more stable polymer−brine−sandstone system which translates into a higher MEB and less polymer adsorption. Figure 11b presents the results of varying NaCl salinities between 15 and 100 g/L on the adsorption and energy barrier at 30 and 90 °C. The disjoining pressure and interaction potential energy curves calculated at 90 °C are shown in Figure 12, where the interaction potential energy curve shifts lower as the brine salinity increases. It can be observed from Figure 11b that the increase in salinity has a condescending effect on the energy barrier and ascending one on adsorption. This can be attributed to the higher negative surface charge screening

https://doi.org/10.1021/acs.energyfuels.3c00542
Energy Fuels XXXX, XXX, XXX−XXX

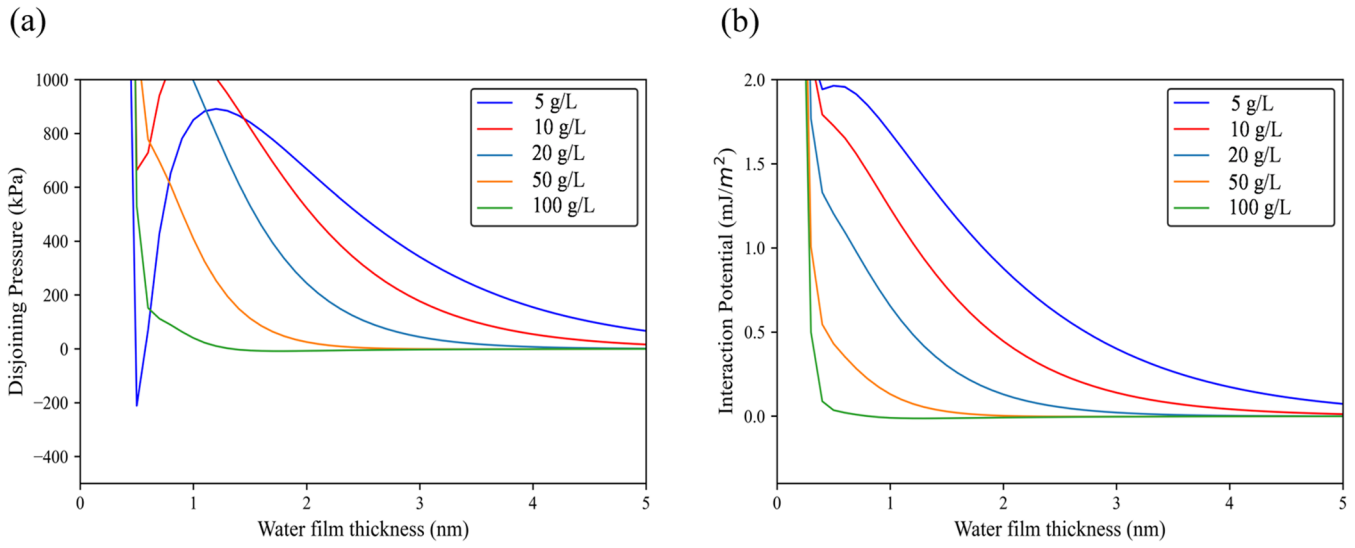

Figure 12. (a) Disjoining pressure and (b) interaction potential energy curves for the HPAM polymer−brine−rock system at 90 °C at various brine salinities.

expected with the increase in the positive sodium ion concentration in the electrolyte. Higher charge screening leads to less repulsion between the polymer and sandstone surface causing the energy barrier to drop and the adsorption to grow, which is in line with previous experimental studies.[58−60] The synergic effects of temperature and salinity can also be evaluated by comparing the curves of 30 and 90 °C temperatures. Whereas at 90 °C, the high temperature progressively suppresses the effect of salinity as it increases in comparison with the 30 °C curves. Hence at 90 °C, the system is more stable over the studied range of salinity as the maximum energy barrier is higher than that of 30 °C leading to lower polymer adsorption at higher temperatures.

4. CONCLUSIONS

In this work, a novel triple-layer surface complexation model was proposed to describe the interactions within the HPAM polymer−brine−sandstone rock system. The developed TLM was employed in tandem with the DLVO theory to investigate the relationship between the rheological properties and interfacial properties of the polymer. Analyzing the ζ potential values predicted from the developed polymer−brine TLM with polymer viscosity measurements adopted from the literature review, showed that polymer solution viscosity and ζ potential are potentially inherently correlated. It was observed that the increase in salinity and decrease in polymer concentration leads to a lower negative charge and ζ potential at the end of the polymer chains resulting in lower chain expansion and consequently lower viscosity. Moreover, the increase in temperature shifts the ζ potential towards more negative values and also decreases the polymer's viscosity. And because ζ potential dictates the wettability alteration due to low-salinity brine injection, it is important to evaluate the effects of salinity, polymer concentration, and temperature on both ζ potential and viscosity prior to low-salinity polymer flooding applications.

The correlation between the polymer adsorption and the maximum energy barrier was evaluated. Results of the analysis showed that the maximum energy barrier can indeed be used to predict polymer adsorption on the rock surface. Analysis of the factors controlling the polymer adsorption using the maximum energy barrier concept leads to the conclusion that higher salinity and lower temperature results in higher polymer adsorption. This is explained by the reduction in the energy barrier when higher brine salinity and lower temperature are encountered, which results in lower system stability leading to higher attraction between the polymer chains and the rock surface. The workflow developed in this study should lend itself to better grasping the control of interfacial interactions within a polymer−brine−rock system that govern the HPAM polymer rheological properties for enhanced oil recovery applications.

AUTHOR INFORMATION

Corresponding Author

Prashant Jadhawar − *School of Engineering, University of Aberdeen, Aberdeen AB24 3UE Scotland, U.K.*; orcid.org/0000-0002-2049-0460; Phone: +44-1244-274180; Email: Prashant.Jadhawar@abdn.ac.uk

Author

Motaz Saeed − *School of Engineering, University of Aberdeen, Aberdeen AB24 3UE Scotland, U.K.*

Complete contact information is available at: https://pubs.acs.org/10.1021/acs.energyfuels.3c00542

Author Contributions

M.S.: Writing—original draft, visualization, investigation, methodology, software, data curation, and formal analysis. P.J.: Supervision, conceptualization, visualization, writing—review and editing, and formal analysis.

Notes

The authors declare no competing financial interest.

REFERENCES

(1) Pourafshary, P.; Moradpour, N.Hybrid EOR Methods Utilizing Low-Salinity Water. In *Enhanced Oil Recovery Processes - New Technologies*; IntechOpen Limited, 2019; Vol. 8, p 25. Jul 8

(2) Sheng, J. J. Critical review of low-salinity waterflooding. *J. Pet. Sci. Eng.* **2014**, *120*, 216−224.

https://doi.org/10.1021/acs.energyfuels.3c00542
Energy Fuels XXXX, XXX, XXX−XXX

(3) Katende, A.; Sagala, F. A critical review of low salinity water flooding: Mechanism, laboratory and field application. *J. Mol. Liq.* **2019**, *278*, 627−649.
(4) Bartels, W. B.; Mahani, H.; Berg, S.; Hassanizadeh, S. M. Literature review of low salinity waterflooding from a length and time scale perspective. *Fuel* **2019**, *236*, 338−353. Jan 15
(5) Tetteh, J. T.; Brady, P. V.; Ghahfarokhi, R. B. Review of low salinity waterflooding in carbonate rocks: mechanisms, investigation techniques, and future directions. *Adv. Colloid Interface Sci.* **2020**, *284*, No. 102253.
(6) Austad, T.Water-Based EOR in Carbonates and Sandstones: New Chemical Understanding of the EOR Potential Using "Smart Water". In *Enhanced Oil Recovery Field Case Studies*; Elsevier, 2013; pp 301−335. Jan 1
(7) Lager, A.; Webb, K. J.; Black, C. J.; Singleton, M.; Sorbie, K. S. In *Low Salinity Oil Recovery-An Experimental Investigation1*, Petrophysics-The SPWLA Journal of Formation Evaluation and Reservoir Description, 2008; 49.
(8) Nasralla, R. A.; Nasr-El-Din, H. A. Double-layer expansion: is it a primary mechanism of improved oil recovery by low-salinity waterflooding? *SPE Reservoir Eval. Eng.* **2014**, *17*, 49−59. Feb 25
(9) Tang, G. Q.; Morrow, N. R. Influence of brine composition and fines migration on crude oil/brine/rock interactions and oil recovery. *J. Pet. Sci. Eng.* **1999**, *24*, 99−111. Dec
(10) Ligthelm, D. J.; Gronsveld, J.; Hofman, J. P.; Brussee, N. J.; Marcelis, F.; Van der Linde, H. A. In *Novel Waterflooding Strategy by Manipulation of Injection Brine Composition*, EUROPEC/EAGE conference and exhibition; OnePetro, 2009.
(11) Jiang, H.; Nuryaningsih, L.; Adidharma, H. In *The Effect of Salinity of Injection Brine on Water Alternating Gas Performance in Tertiary Miscible Carbon Dioxide Flooding: Experimental Study*, SPE Western Regional Meeting; OnePetro, 2010.
(12) Aleidan, A.; Mamora, D. D. In *SWACO2 and WACO2 Efficiency Improvement in Carbonate Cores by Lowering Water Salinity*, Society of Petroleum Engineers - Canadian Unconventional Resources and International Petroleum Conference, 2010; pp 1633−1647.
(13) Kumar, H. T.; Shehata, A. M.; Nasr-El-Din, H. A. *Effectiveness of low-salinity and CO2 flooding hybrid approaches in low-permeability sandstone reservoirs*, Society of Petroleum Engineers - SPE Trinidad and Tobago Section Energy Resources Conference, 2016.
(14) Teklu, T. W.; Alameri, W.; Graves, R. M.; Kazemi, H.; AlSumaiti, A. M. Low-salinity water-alternating-CO2 EOR. *J. Pet. Sci. Eng.* **2016**, *142*, 101−118. Jun 1
(15) Alameri, W.; Teklu, T.; Graves, R.; Kazemi, H.; AlSumaiti, A. *Low-salinity Water-alternate-surfactant in Low-permeability Carbonate Reservoirs*, IOR 2015 − 18th European Symposium on Improved Oil Recovery, 2015.
(16) Jha, N. K.; Lebedev, M.; Iglauer, S.; Ali, M.; Roshan, H.; Barifcani, A.; et al. Pore scale investigation of low salinity surfactant nanofluid injection into oil saturated sandstone via X-ray micro-tomography. *J. Colloid Interface Sci.* **2020**, *562*, 370−380. Mar 7
(17) Kumar, G.; Behera, U. S.; Mani, E.; Sangwai, J. S. Engineering the Wettability Alteration of Sandstone Using Surfactant-Assisted Functional Silica Nanofluids in Low-Salinity Seawater for Enhanced Oil Recovery. *ACS Eng. Au* **2022**, *2*, 421−435. May 6
(18) Green, D. W.; Willhite, G. P. Enhanced Oil Recovery. In *Society of Petroleum Engineers*; OnePetro, 2018.
(19) Jadhawar, P.; Saeed, M. Low Salinity Waterflooding and Polymer Enhanced Oil Recovery from Sandstone reservoirs. In *DEVEX 2019 - Legacy & Sustainability: 50+ Years of UKCS History and Lessons for the Future*; SPE Aberdeen: Aberdeen, United Kingdom, 2019.
(20) Jadhawar, P.; Saeed, M. Low salinity water and polymer flooding in sandstone reservoirs: Upscaling from nano-to macro-scale using the maximum energy barrier. *J. Pet. Sci. Eng.* **2023**, *220*, No. 111247. Jan 1
(21) Kozaki, C. Efficiency of Low Salinity Polymer Flooding in Sandstone Cores, MSc Dissertation, University of Texas at Austin, 2012.
(22) Shiran, B. S.; Skauge, A. Enhanced oil recovery (EOR) by combined low salinity water/polymer flooding. *Energy Fuels* **2013**, *27*, 1223−1235. Mar 21
(23) Al Sofi, A. M.; Wang, J.; Al Boqmi, A. M.; Al Otaibi, M. B.; Ayirala, S. C.; Al Yousef, A. A. In *SmartWater Synergy with Chemical EOR for a Slightly Viscous Arabian Heavy Reservoir*, Society of Petroleum Engineers - SPE Heavy Oil Conference and Exhibition, 2016.
(24) Almansour, A. O.; AlQuraishi, A. A.; AlHussinan, S. N.; AlYami, H. Q. Efficiency of enhanced oil recovery using polymer-augmented low salinity flooding. *J. Pet. Explor. Prod. Technol.* **2017**, *7*, 1149−1158. Dec 1
(25) Torrijos, I. D. P.; Puntervold, T.; Strand, S.; Austad, T.; Bleivik, T. H.; Abdullah, H. I. An experimental study of the low salinity Smart Water - Polymer hybrid EOR effect in sandstone material. *J. Pet. Sci. Eng.* **2018**, *164*, 219−229. May 1
(26) Tahir, M.; Hincapie, R. E.; Foedisch, H.; Abdullah, H.; Ganzer, L. In *Impact of Sulphates Presence During Application of Smart Water Flooding Combined with Polymer Flooding*, Society of Petroleum Engineers - SPE Europec featured at 80th EAGE Conference and Exhibition, 2018.
(27) Unsal, E.; ten Berge, A. B. G. M.; Wever, D. A. Z. Low salinity polymer flooding: Lower polymer retention and improved injectivity. *J Pet Sci Eng.* **2018**, *163*, 671−682. Apr 1
(28) Kakati, A.; Kumar, G.; Sangwai, J. S. Low salinity polymer flooding: effect on polymer rheology, injectivity, retention, and oil recovery efficiency. *Energy Fuels* **2020**, *34*, 5715−5732. Apr 20
(29) Sarvestani, A. D.; Rostami, B.; Mahani, H. Polymer-Enhanced Low-Salinity Brine to Control In Situ Mixing and Salt Dispersion in Low-Salinity Waterflooding. *Energy Fuels* **2021**, *35*, 10540−10550. Jun 16
(30) Kamal, M. S.; Sultan, A. S.; Al-Mubaiyedh, U. A.; Hussein, I. A. Review on polymer flooding: Rheology, adsorption, stability, and field applications of various polymer systems. *Polym. Rev.* **2015**, *55*, 491−530. Jul 3
(31) Algharaib, M.; Alajmi, A.; Gharbi, R. Improving polymer flood performance in high salinity reservoirs. *J. Pet. Sci. Eng.* **2014**, *115*, 17−23. Mar 1
(32) Brown, R. S.; Bennet, A. J.; Slebocka-Tilk, H. Recent perspectives concerning the mechanism of H3O+-and hydroxide-promoted amide hydrolysis. *Acc. Chem. Res.* **1992**, *25*, 481−488. Nov 1
(33) Sheng, J. *Modern Chemical EOR-Theory and Practice*; Elsevier, 2010.
(34) Luo, J. H.; Liu, Y. Z.; Zhu, P. Polymer Solution Properties and Displacement Mechanisms. In *Enhanced Oil Recovery-Polymer Flooding*; Shen, P.-P.; Liu, Y.-Z.; Liu, H.-R., Eds.; Petroleum Industry Press: Beijing, 2006; pp 1−72.
(35) Lee, S. J. *Development of a Comprehensive Rheological Property Database for EOR Polymers*; University of Texas at Austin, 2009.
(36) Mandal, A.; Ojha, K. In *Optimum Formulation of Alkaline-Surfactant-Polymer Systems for Enhanced Oil Recovery*, SPE Asia Pacific Oil and Gas Conference and Exhibition; OnePetro, 2008.
(37) Lee, S.; Kim, D. H.; Huh, C.; Pope, G. A. In *Development of a Comprehensive Rheological Property Database for EOR Polymers*, SPE Annual Technical Conference and Exhibition; OnePetro, 2009.
(38) Tam, K. C.; Tiu, C. Role of ionic species and valency on the steady shear behavior of partially hydrolyzed polyacrylamide solutions. *Colloid Polym. Sci.* **1990**, *268*, 911−920. Oct
(39) Choi, B.; Jeong, M. S.; Lee, K. S. Temperature-dependent viscosity model of HPAM polymer through high-temperature reservoirs. *Polym. Degrad. Stab.* **2014**, *110*, 225−231. Dec 1
(40) Luo, W.; Xu, S. In *Chemical Degradation of HPAM by Oxidization in Produced Water: Experimental Study*, SPE Americas E&P Health, Safety, Security and Environmental Conference; OnePetro, 2013.
(41) Gao, C. Viscosity of partially hydrolyzed polyacrylamide under shearing and heat. *J. Pet. Explor. Prod. Technol.* **2013**, *3*, 203−206. Sep

https://doi.org/10.1021/acs.energyfuels.3c00542
Energy Fuels XXXX, XXX, XXX−XXX

(42) Zaitoun, A.; Potie, B. In *Limiting Conditions for the Use of Hydrolyzed Polyacrylamides in Brines Containing Divalent Ions*, SPE Oilfield and Geothermal Chemistry Symposium; OnePetro, 1983.
(43) Chiappa, L.; Mennella, A.; Lockhart, T. P.; Burrafato, G. Polymer adsorption at the brine/rock interface: the role of electrostatic interactions and wettability. *J. Pet. Sci. Eng.* **1999**, *24*, 113−122. Dec 1
(44) Katz, L. E.; Hayes, K. F. Surface complexation modeling: II. Strategy for modeling polymer and precipitation reactions at high surface coverage. *J. Colloid Interface Sci.* **1995**, *170*, 491−501. Mar 15
(45) Saha, B.; Streat, M. Adsorption of trace heavy metals: Application of surface complexation theory to a macroporous polymer and a weakly acidic ion-exchange resin. *Ind. Eng. Chem. Res.* **2005**, *44*, 8671−8681. Nov 9
(46) Saeed, M.; Jadhawar, P.; Ayirala, S. C.; Abhishek, R.; Zhou, Y. Modelling the effects of reservoir parameters and rock mineralogy on wettability during low salinity waterflooding in sandstone reservoirs. *J. Pet. Sci. Eng.* **2022**, *215*, No. 110676. Aug 1
(47) Vieira, A. R. *Surface Complexation Modeling of Lead (II), Cadmium (II) and Selenium (IV) onto Iron Hydroxides in Single and Bisolute Systems*; The University of Texas at Austin, 2006.
(48) Villalobos, M. Triple Layer Modelling of Carbonate Adsorption on Goethites with Variable Adsorption Capacities Based on Congruent Site-Occupancy. In *Interface Science and Technology*; Elsevier, 2006; Vol. *11*, pp 417−442.
(49) Hiemstra, T.; Van Riemsdijk, W. H. A surface structural approach to ion adsorption: the charge distribution (CD) model. *J. Colloid Interface Sci.* **1996**, *179*, 488−508. May 10
(50) Al-Busaidi, I. K.; Al-Maamari, R. S.; Al Mahrouqi, D.; Karimi, M. Impact of polymer on electro-kinetic properties of crude oil, brine and rock interfaces. *J. Pet. Sci. Eng.* **2022**, *213*, No. 110390. Jun 1
(51) Saeed, M.; Jadhawar, P.; Zhou, Y.; Abhishek, R. Triple-layer surface complexation modelling: Characterization of oil-brine interfacial zeta potential under varying conditions of temperature, pH, oil properties and potential determining ions. *Colloids Surf., A* **2022**, *633*, No. 127903. Jan 20
(52) Pourakaberian, A.; Mahani, H.; Niasar, V. The impact of the electrical behavior of oil-brine-rock interfaces on the ionic transport rate in a thin film, hydrodynamic pressure, and low salinity waterflooding effect. *Colloids Surf., A* **2021**, *620*, No. 126543. Jul 5
(53) Israelachvili, J. N. *Intermolecular and Surface Forces*; Academic Press, 2011.
(54) Gregory, J. Approximate expressions for retarded van der Waals interaction. *J. Colloid Interface Sci.* **1981**, *83*, 138−145. Sep 1
(55) Hirasakl, G. J. Wettability: fundamentals and surface forces. *SPE Form. Eval.* **1991**, *6*, 217−226.
(56) Page, M.; Lecourtier, J.; Noïk, C.; Foissy, A. Adsorption of polyacrylamides and of polysaccharides on siliceous materials and kaolinite: influence of temperature. *J. Colloid Interface Sci.* **1993**, *161*, 450−454. Dec 1
(57) Ewoldt, R. H.; Johnston, M. T.; Caretta, L. M. *Complex Fluids in Biological Systems. Biological and Medical Physics, Biomedical Engineering*; Springer: New York, 2015; pp 207−241.
(58) Wiśniewska, M. The temperature effect on the adsorption mechanism of polyacrylamide on the silica surface and its stability. *Appl. Surf. Sci.* **2012**, *258*, 3094−3101. Jan 15
(59) Lu, J. H.; Wu, L.; Letey, J. Effects of soil and water properties on anionic polyacrylamide sorption. *Soil Sci. Soc. Am. J.* **2002**, *66*, 578−584.
(60) Bessaies-Bey, H.; Fusier, J.; Harrisson, S.; Destarac, M.; Jouenne, S.; Passade-Boupat, N.; Lequeux, F.; de Lacaillerie, J. B.; Sanson, N. Impact of polyacrylamide adsorption on flow through porous siliceous materials: State of the art, discussion and industrial concern. *J. Colloid Interface Sci.* **2018**, *531*, 693−704. Dec 1

https://doi.org/10.1021/acs.energyfuels.3c00542
Energy Fuels XXXX, XXX, XXX−XXX